AIAA JOURNAL
Vol. 43, No. 8, August 2005

Microgravity Laminar Diffusion Flame in a Perpendicular Fuel and Oxidizer Stream Configuration

L. Brahmi,* T. Vietoris,* S. Rouvreau,† and P. Joulain‡
Ecole Nationale Supérieure de Mécanique et d'Aérotechniques, 86960 Futuroscope-Chasseneuil du Poitou Cedex, France
L. David§
Université de Poitiers, 86962 Futuroscope-Chasseneuil du Poitou Cedex, France
and
J. L. Torero¶
University of Edinburgh, Edinburgh, Scotland EH9 3JN, United Kingdom

Fuel is injected through a porous flat plate perpendicular to a stream of oxidizer flowing parallel to the surface of the burner for regimes corresponding to a fire scenario in spacecrafts. Particle image velocimetry is used to characterize the flow structure in nonreactive conditions. The influence of fuel injection on the flow structure is evaluated, and a detailed description of the flow structure is presented. For combustion experiments, a minimum fuel injection velocity is shown to be necessary for a stable flame. The influence of thermal expansion on the flame is evaluated. A complementary numerical study is used to support the preceding experimental observations.

Introduction

MOTIVATED by fire safety concerns and the advent of long-term microgravity facilities, a renewed interest in fire propagation at very low Reynolds numbers [$Re < 10^2$ is typical of spacecraft heat-ventilation- and-air-conditioning (HVAC) systems] has arisen in the past two decades.[1] The current status of fire safety practices in different existing and planned space facilities has been addressed by many authors,[1–6] and recent related progress has been summarized in Refs. 7 and 8. These studies show a need for fundamental combustion studies in microgravity to properly establish fire safety protocols in environments that become every day more challenging.

A common fire scenario is that of a burning condensed fuel. Condensed combustible material often burn such that a diffusion flame establishes over its surface. If the oxidizer flows parallel to the combustible surface, a stationary diffusion flame will establish in the boundary layer generated over the fuel. Heat transfer from the flame to the surface vaporizes the condensed fuel, which is transported toward the flame by convection and diffusion. When the fuel reaches the flame, it exothermically reacts with the oxidizer and provides the necessary heat to sustain further pyrolysis.

In normal gravity, temperature gradients result in natural convective flows that are laminar when the scale is small and transition to turbulence as the size of the fuel increases. In spacecraft, where buoyancy is negligible, the flow is limited to that induced by external forced advections. Characteristic velocities of HVAC systems are of the order of 0.1 m/s; therefore, the flow is expected to be laminar. The complex mixed flow (often turbulent) fire scenario observed in normal gravity is reduced to the classical combustion problem first described by Emmons.[9] The problem of a chemically reacting boundary-layer flow over a flat plate, as described by Emmons, is that of the incompressible boundary-layer flow with blowing. The assumptions correspond to a classical Shvab–Zeldovich approach where gravity is neglected.

Extensive research has been done following this pioneering work to use the theoretical framework to explain different fire scenarios. The natural constraints imposed by buoyancy and the differences between normal gravity fires and the laminar diffusion flame studied by Emmons have prevented complete validation of this model. Despite this fact, many studies have made boundary-layer assumptions to study different aspects of the problem such as flame spread[10] or flame length.[11] Perturbations on the classical boundary-layer solution have added the effect of buoyancy[12,13] and recognized the elliptic nature of the Navier–Stokes equations close to the leading edge.[14–16] Experimental work that serves to validate the original assumptions of Emmons[9] is, to the best knowledge of the authors, not available. The limiting factors are buoyancy and fuel surface regression that create an inherently unsteady problem. Coupling between heat feedback from the flame, fuel supply, buoyancy, and flame geometry create an insurmountable gap between experiments and the theoretical assumptions of Emmons.

A number of notable attempts to approach the theoretical assumptions can be found in the literature. Of relevance to this work are studies in which porous burners have been used. Porous burners have been used regularly in an attempt to simplify experiments. If a gas is used as fuel, the coupling between heat feedback from the flame and fuel supply is circumvented, and different fuels can be simulated just by changing the mass transfer number.[17,18] If the combustible is a liquid, then convection inside the fuel bed is precluded. In both cases the regression problem is avoided, and longer experimentation time can be achieved. Following this methodology, the gas phase can be studied without incorporating into the experiments the characteristics of the condensed-phase pyrolysis.

Numerous studies have used this type of burners to address turbulent flames typical of fire scenarios and have been summarized by Drysdale.[17] Laminar diffusion flame studies are not as common. Most of the work in this area concentrated on the description and explanation of velocity overshoots close to the reacting zone and their effect on flame stability. The experimental conditions at Earth gravity were defined to minimize the effect of buoyancy; therefore, the horizontal configuration was preferred, and freestream velocities were generally of the order of 1 m/s.

The first to observe velocity overshoots near the reaction zone were Hirano et al.[19] and Hirano and Kanno.[20] Pressure fields were

Received 15 September 2004; revision received 8 March 2005; accepted for publication 29 March 2005.

*Research Fellow, Laboratoire de Combustion et de Détonique, 2 Avenue Clément Ader, B.P. 109, Téléport 2.
†Research Fellow, Laboratoire de Combustion et de Détonique, 2 Avenue Clément Ader, B.P. 109, Téléport 2; seb.rouvreau@tele2.fr
‡Professor, Laboratoire de Combustion et de Détonique, 2 Avenue Clément Ader, B.P. 109, Téléport 2.
§Lecturer, Laboratoire d'Etude Aérodynamique, UMR6609, SP2MI, Téléport 2, Boulevard Marie et Pierre Curie, B.P. 30179.
¶Assistant Professor, School of Engineering and Electronics.

calculated from the velocity measurements and showed distortions near the leading edge. The experiments were conducted using a porous plate through which a liquid or gaseous fuel was injected, and the forced flow velocity ranged between 0.2 and 1.4 m/s. They concluded that the velocity overshoots occur because of thermally induced pressure gradients. Ramachandra and Raghunandan,[21] on a similar burner, studied the effect of injection and freestream velocities on the stability of vaporized n-heptane flames and provided similar explanations to those proposed by Hirano et al.[19] and Hirano and Kanno.[20] It was also suggested that the confined nature of their experimental facility (50×130 mm) resulted in a favorable pressure gradient and acceleration of the flow. They observed that the magnesium-oxide particles used to seed the oxidizer stream could not cross the flame; thus, velocity measurements could not be made below the flame.

Lavid and Berlad,[12] in a theoretical study, attributed the pressure overshoots to buoyancy and defined nondimensional length scales that incorporated the Grashoff number and serve to describe buoyantly induced perturbations in the pressure field. Andreussi and coworkers.[22–24] incorporated variable properties to a theoretical analysis very similar to that of Emmons[22,23] and compared a numerical solution to experiments conducted with ethyl alcohol.[22,24] They concluded that the Shvab–Zeldovich formulation is only adequate for freestream velocities higher than 1.2 m/s. For slower flows, velocity overshoots appear, and the authors attribute them to buoyancy. They add that the first-order approximation proposed by Lavid and Berlad[12] is not sufficient to describe these overshoots. Further refinement of the gas-phase properties was obtained by including thermal cracking of the fuel.[25] Introduction of exact physical properties resulted in improved accuracy for numerical temperature calculations. Although improper definition of the gas-phase properties was then argued as the cause of the velocity overshoots, no velocity distributions were presented in this work.

A different approach to explaining the discrepancies between the different experimental studies was followed by Ha et al.[26] A study of the leading edge was conducted in an attempt to provide a conciliating explanation to the velocity overshoots. Cold and reacting flow velocity measurements and flow visualization together with elliptic numerical calculations were used to describe the separation close to the leading edge. As in the work of Hirano et al.[19] and Hirano and Kanno,[20] cold-flow velocities were measured without fuel injection. The authors argued that the different geometries used by the different studies lead to different experimental results. A leading-edge extension plate precludes flow separation and results in a local acceleration that leads to velocity overshoots that are only evident for freestream velocities of the order of 1 m/s. These overshoots can be predicted by their numerical model and describe well the observations of Hirano et al.,[19] Hirano and Kanno,[20] and Ramachandra and Raghunandan.[21] Without the extension plate, velocity overshoots occur earlier as a result of the interaction between the flame and the separation flow.

The studies just mentioned have used airflow velocities of the order of 1 m/s in an attempt to escape the effects of buoyancy. A study, of similar nature, conducted by Torero et al.[27,28] extended the range of velocities explored by previous investigators.[19–26] By conducting experiments under microgravity conditions, the dominant effect of buoyancy was avoided, and freestream velocities below 0.2 m/s could be studied. Ethane injected through a sintered bronze plate simulated the combustible fuel and showed that for velocities of the order of 0.1 m/s the flame standoff distance is an order of magnitude larger than that predicted by a Shvab–Zeldovich analysis.[29] The authors explained the unexpected flame geometry on the structure of the flow, but lack of velocity measurements precluded complete verification of their hypotheses.

These studies provide conclusive evidence of perturbations on the flow occurring during the combustion process, but the explanations for these overshoots are not consistent among themselves. Although of great relevance to the nature of the flames, none of the just-described studies presents a systematic evaluation of the effect of fuel injection on the characteristics of the oxidizer flow. In this work, a study of the nonreacting flow structure above a porous gas burner is conducted to extend the preliminary work of Torero et al.[27,29] The freestream velocity is adjusted to keep the Reynolds number below 800, and the fuel injection velocity is kept below 10 mm/s. The choice of freestream and fuel-injection velocities is consistent with the spacecraft fire application. Flow visualization with a light sheet and independent seeding of fuel and oxidizer is used to describe the nature of the interaction between fuel and oxidizer flows. Visualization and particle image velocimetry are conducted with nonreacting flow to determine the characteristics of the mixing zone. Reacting flow experiments are conducted in microgravity using a 2.2-s. drop tower and parabolic flights. The parameters varied are the oxidizer concentration and fuel and freestream velocities. Numerical simulations complement the experimental study. A full description of both the code[30] and these computations[31] have been published elsewhere and will not be repeated here.

Experimental Setup

Combustion Facility

A gas burner is placed in the center of a combustion chamber of 320 mm in diameter and 400 mm in total length. A schematic of the experimental hardware is shown in Fig. 1. The hardware was designed to be used at drop towers and parabolic flights, and therefore is fully automated and leak proof.

The burner is a 200×95 mm stainless-steel plate with an aerodynamic leading edge to prevent separation of the boundary layer. A $60 \times 60 \times 5$ mm-thick sintered bronze plate is placed 40 mm behind the leading edge and centered in the burner plate. The distance from the leading edge of the burner to the leading edge of the porous plate was chosen to prevent separation and based on the work of Ha et al.[26] The surface of the sintered bronze is flush with the burner surface and covers a small chamber where a sintered bronze disk (10 mm in diameter and 5 mm thick) serves as inlet for the gas flow.

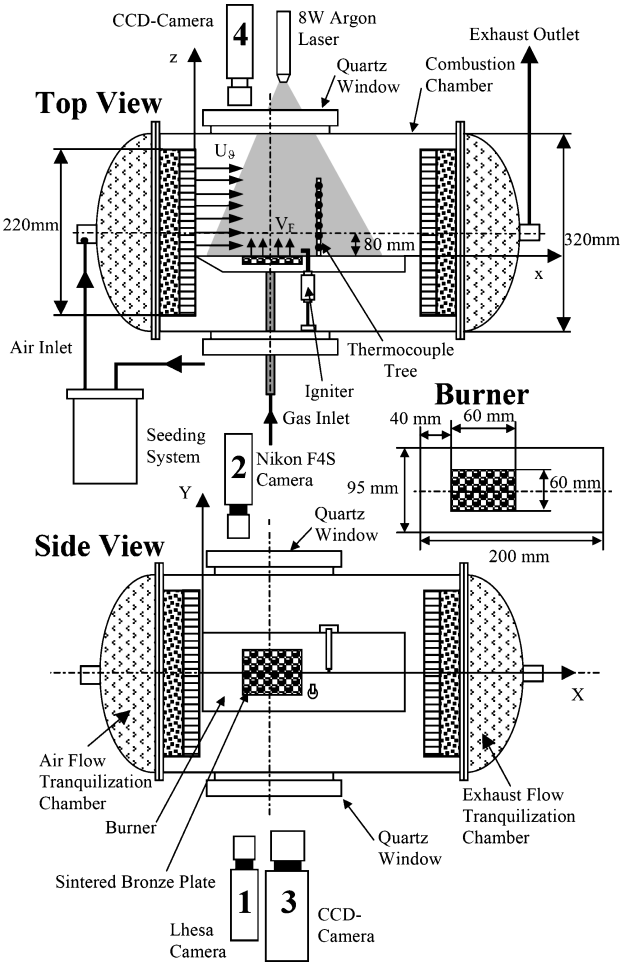

Fig. 1 Schematic of the experimental apparatus.

The inlet is placed behind the trailing edge of the burner to guarantee a homogeneous flow out of the porous plate. The pore diameter and plate size were selected to guarantee a one-dimensional flow of fuel at the surface of the porous plate. Characterization of the flow without injection showed a two-dimensional boundary layer that corresponded well with classic theoretical predictions[32] forming over the entire surface of the burner.

The fuel is introduced into the burner through a controlled mass flowmeter with a characteristic velocity V_F. The characteristic velocity is obtained from the controlled mass flowmeter and corresponds well with hot-wire anemometer measurements done to characterize the homogeneity of the flow above the burner. A spark plug is placed at the trailing edge of the porous plate, flush with the burner surface to minimize flow perturbations. The spark is controlled automatically through the data acquisition and control system and serves as igniter. The burner and sintered bronze plate were blackened to minimize reflection.

A thermocouple tree is attached to one side of the burner 10 mm behind the trailing edge of the porous plate. The thermocouple tree consists of eight type K thermocouples with beads 25 μm in diameter. The beads are placed at the axis of symmetry of the burner and at a vertical distance of 2, 5, 10, 15, 23, 31, 41, and 53 mm from the burner surface. Because of the high stresses imposed by microgravity facilities (landing in the drop tower and vibrations in the aircraft), the thermocouples had to be cased in a stainless-steel sheath of 1-mm external diameter. The thermocouples imposed significant perturbations on the flow and, therefore, were only used for characteristic experiments. Flame quenching occurs around the stainless-steel sheet. Quenching is not obvious close to the thermocouple tip; therefore, it can be considered that the thermocouples provide an adequate characteristic temperature for the flame. Although corrected for radiative losses, the thermocouple measurements are only expected to provide an indication of the relative temperature changes occurring under different experimental conditions; therefore, the temperatures presented throughout this work should not be considered as actual flame temperatures.

The flow is introduced through a cylindrical section 220 mm in diameter. The size of the chamber and air inlet guarantees a one-dimensional flow where the burner will be placed. Oxidizer velocities U_∞ are controlled by means of mass flowmeters. The oxidizer flow enters and exits the combustion chamber through its main axis (x coordinate), fuel is injected perpendicular to the oxidizer flow (z coordinate), and y is the coordinate perpendicular to the plane established by both flows. The cylindrical inlet section consists of a series of honeycomb plates in order to obtain a constant velocity in a section that exceeds the burner dimension ($\phi > 120$ mm). Details on the particles used for seeding will be provided in the next section. A similar section is placed at the trailing edge of the burner to exhaust the gases. Characterization of the homogeneity of the flow in the chamber was done by using a hot-wire anemometer. Characterization was done with and without the burner and in all cases with no injection through the porous plate.

The maximum dimensions for the combustion chamber were determined by the constraints imposed by the drop tower (drop capsule of 0.8 m in diameter). All other dimensions had to be scaled based on these criteria. The burner and injection plate size were chosen to guarantee that the combustion chamber acts as infinitely far boundary to avoid perturbations as those observed by Ramachandra and Raghunandan[21] and Torero et al.[27] The width of the injection plate was chosen to minimize burner edge effects affecting the flow in the area above the sintered bronze. As mentioned before, all of these considerations correspond to the no-injection condition ($V_F = 0$).

Experiments were conducted at Earth gravity for the nonreactive flow, at the 2.2-s. drop tower at the Instituto Nacional de Tecnica Aeroespacial (INTA) and onboard the NASA-KC-135 and CNES-Caravelle and Airbus A300 aircraft for the reactive flow. The drop tower provided microgravity levels of $10^{-4} g_0$, and the aircraft allowed for 25 s of experimentation at microgravity levels of 10^{-2}–10^{-3} g_0 ($g_0 = 9.81$ m/s^2).

The different facilities were used to optimize the microgravity time. Velocities in the upper range correspond to the shortest transition times; therefore, drop towers were preferred for these conditions. Slower flows required longer times to attain steady-state conditions; therefore, 25-s parabolas were preferred for these experiments. A compromise was necessary because perturbations in the gravity level affected mostly the low flow conditions. Therefore, for experiments with low flow conditions or close to extinction conditions tests were conducted using both facilities and the results compared.

Flow Visualization

A light sheet originating from an 8-W argon laser (514 nm) is introduced from the $-z$ direction. The light sheet is parallel to the x–z plane, and its position can be varied in the x and y directions.

Seeding of the flow is accomplished by means of incense smoke (particle size of the order of 1 μm) or oil (average particle size 10 μm) to avoid clogging. The choice on how fuel and air are introduced into the chamber is determined by the constraints imposed by microgravity facilities.

Ethane ($\rho = 1.25$ kg/m^3) was used as fuel and mixtures of oxygen ($\rho = 1.33$ kg/m^3) and nitrogen ($\rho = 1.17$ kg/m^3) as oxidizer. The similar density and viscosity of fuel and oxidizer allows the use of only air ($\rho = 1.21$ kg/m^3) for nonreacting flow visualization; For convenience, in all cases presented the main stream will be referred as oxidizer and the gas injected through the porous plate as fuel.

An intensified LHESA video camera (25 frames per second), camera 1 on Fig. 1, and a Nikon F4S camera (camera 2) are used to capture the necessary images for particle induced velocimetry (PIV) and flow visualization, respectively. A charge-coupled-device (CCD)-HI8-Hitachi camera (camera 3) provides the side view of the visible flame, and a Sony XC-999P high-resolution (752 × 582 pixels) black and white camera (camera 4) is used to record the top view.

Image Processing

Images are recorded to Hi-8 video tapes and processed a posteriori to provide a better presentation. Image acquisition is done by means of a Miro-DC30 card that captures sequences of 25 images with a resolution of 786 × 576 pixels. Flow-visualization images are digitalized, the contrast enhanced, and whenever necessary light reflection from the burner eliminated.

Image processing and treatment to obtain the velocity distributions followed the methodology described in detail by David.[33] PIV treatment based on the binary image method developed by David et al.[34] is employed for this work.

For this particular application, the time separating each image is defined as $\Delta t = 1/25$ s, and the correlations were conducted on images with 80-ms intervals.

Experimental Conditions

For the study of reactive flows, ethane was injected through the burner, and experiments were conducted under normal and microgravity conditions. For the present flow conditions, the effect of buoyancy is overwhelming,[29] and all resemblance to a reactive boundary-layer flow is lost: therefore, only experiments conducted in microgravity will be presented here.

The flame luminosity was extracted by means of image processing of the video recordings. Once the images were digitalized to gray levels that corresponded to values ranging from 0 to 256 (0 corresponds to black and 256 to white), and the flame boundary was established when a discontinuity in the gray level was observed. In most cases this boundary corresponded to a drastic change in color (blue to yellow), but in some cases, especially close to extinction areas, it represented a sudden decrease in the luminous intensity. The flame geometries presented in the following sections do not correspond to any quantitative representation of the chemical reaction but more to a representative location that will serve as a reference.

Experiments in microgravity have shown that, for low flow velocities, the flame can be almost invisible[5,8] therefore, in some cases the images might lead to the conclusion that the flame is not present in an area where an exothermic chemical reaction is still occurring. This phenomenon seems to occur mostly at the trailing edge of the flame and will be considered as part of the error incurred in this study.

Experiments were conducted for different forced flow velocities ($U_\infty < 150$ mm/s), fuel-injection velocities ($V_F < 10$ mm/s), and oxygen mass fraction ($20\% < Y_O < 55\%$). Dilution is done by means of nitrogen.

Ignition was accomplished in normal and in microgravity conditions with very similar results in both cases. For safety reasons, most experiments were ignited in normal gravity although the transition period between normal and microgravity was longer. Experiments were conducted by placing the burner on both ceiling and floor; it was observed that the ultimate characteristics of the flame were independent of the burner positioning, but that the transition period was shorter in the former case, and thus it was preferred.

General Flame Characteristics

More than 120 experimental conditions were tested in the domain presented in Fig. 2. Three types of flames have been observed depending on the regime: in region 1, regimes where the flame covers the burner with an elliptical shape (Fig. 3a); region 2 concerns flames with a parabolic shape (Fig. 3e); and region 3 concerns flames with a linear shape (Fig. 3f). Data points marked from a to f correspond to the images presented in Fig. 3. The data presented for these cases will be those of a single image that represented best the most repeated position. This treatment was preferred over an average image because the amplitude and irregularity of the perturbations had a tendency to distort the mean value.

Extinction

A minimum fuel injection velocity below which extinction occurred was determined. As this limit was approached, generalized pulsations could be observed before extinction all over the burner surface. For $U_\infty < 70$ mm/s extinction occurred for $V_F < 0.9$ mm/s, and for $U_\infty > 70$ mm/s the extinction limit increased linearly with the freestream velocity (Fig. 2). This extinction limit was mostly independent of the oxygen concentration. For higher injection velocities, the flames were observed to be stable for all oxidizer velocities and oxygen concentrations. No extinction was observed for quiescent conditions ($U_\infty = 0$) because the fuel supply remained constant and the experimental times are short enough to keep the oxygen concentration in the chamber almost invariant. For $U_\infty \approx 120$ mm/s and oxygen concentration, $Y_O = 18\%$, the flame begun to pulsate and became unstable, and the instabilities disappeared for higher oxygen concentrations. In this regime, pulsations were observed only at the leading edge of the burner. Further increase in the velocity lead to the flame being completely blown off. Blowoff extinction in this type of regime has been previously studied in detail[14,16,27] and will therefore not be explored here.

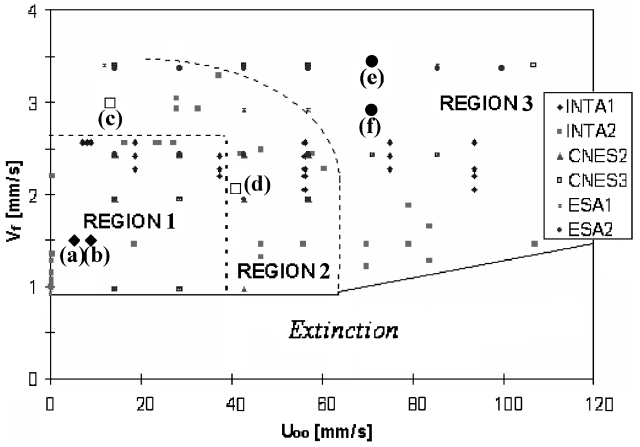

Fig. 2 Characteristic regions for microgravity flames. Experiments presented here come either from drop-tower microgravity campaigns (INTA-Spain) or from parabolic flight campaigns (ESA or Centre National d'Etudes Speciales).

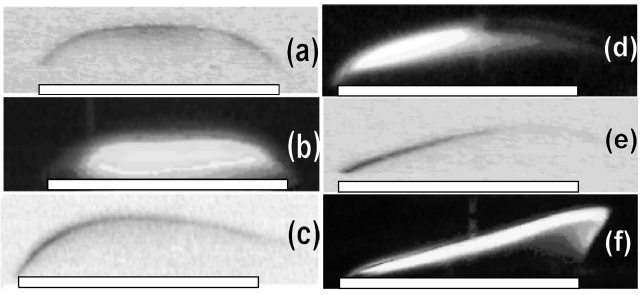

Fig. 3 Photographic images of microgravity flames a), c), and e) $Y_O = 22\%$; b), d), and f) $Y_O = 50\%$. Negative images are presented for $Y_O = 22\%$.

Flame Regimes

Stable flames observed through these experiments can be categorized in three regimes, and a few representative cases have been chosen to illustrate the differences between these three regimes. Still images of a representative flame corresponding to each condition chosen are presented in Fig. 3.

In region 1 the flame covers the entire burner and is flat on top of the burner and almost symmetrical (Figs. 3a and 3b). As the flame exits the burner, it approaches the surface; the quenching distance at the leading and trailing edge is very small and difficult to quantify visually. The flames cover a region that significantly exceeds the burner dimensions in both x and y directions. Figure 3a shows a negative image of a flame where the oxidizer concentration was 22%. Figure 3b shows a case with very similar fuel and oxidizer velocities and oxygen concentration of 50%. The geometrical characteristics of the flame are very similar for both cases showing no influence of the oxygen concentration on the shape of the flame. Superposition of both images shows discrepancies in the standoff distance, especially close to the leading edge.

As flames progress toward region 2, they detach from the trailing edge (Figs. 3c and 3d). The actual detachment might not be real because the CCD camera could not resolve any significant luminous intensity variations in this region. No quantitative data can be extracted from the trailing-edge zone. What is clear is that the leading edge remains attached to the burner surface, upstream of the leading edge of the porous plate. The curvature of the leading edge is more pronounced than the curvature of flames in region 1. Flames in this region are blue close to the leading edge progressing toward yellow further downstream. The flame is not symmetric, and beyond the yellow zone the luminous intensity decreases as x increases. The flames in this region significantly exceed the burner dimensions at the trailing edge. Figure 3c shows the negative of a flame for $Y_O = 22\%$ and Fig. 3d the direct image for $Y_O = 50\%$. Figures 3c and 3d correspond to different flow conditions, and so the geometry is not directly comparable. Instead, the different conditions serve to illustrate that the main geometrical features remain the same independent of the location, within region 2, of the particular experimental conditions.

Region 2 serves as a transition region between regions 1 and 3. Region 3 is characterized by a small blue and curved zone close to the leading edge followed by a linear yellow zone. The flame leading edge is positioned very close to the porous plate edge showing the parabolic nature of this region (Figs. 3e and 3f). The flame is fully detached from the burner, and extinction can be clearly seen at the trailing edge. As for region 2, the flames significantly exceed the burner dimensions at the trailing edge. Figure 3e shows the negative of a flame with $Y_O = 22\%$ and Fig. 3f the direct image when $Y_O = 50\%$. Both cases have very comparable oxidizer and fuel velocities. The oxygen concentration seems to have very little effect on the inclination of the flame close to the leading edge, but toward the trailing edge both flames are significantly different. For lower oxygen concentrations the flames bend earlier and approach the burner surface as the distance downstream increases. For higher oxygen concentrations the flame remains linear and extinguishes abruptly. A top view of the flame showed more clearly the abrupt extinction. The luminous zone descending toward the burner that can be seen in Fig. 3f corresponds to the edges ($\pm y \approx 30$ mm) of the flame.

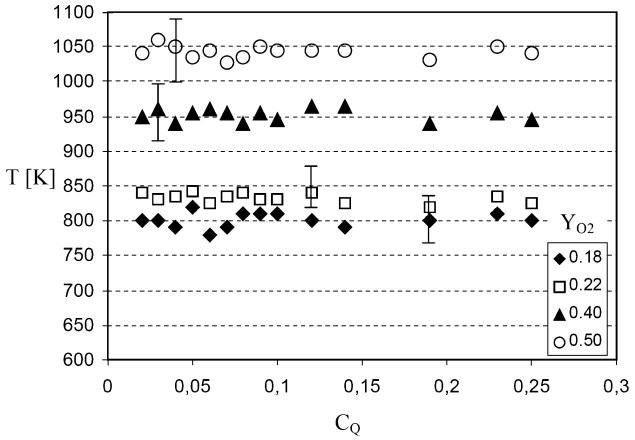

Fig. 4 Characteristic temperature measurements for different oxygen concentrations Y_O and different values of the dimensionless volume coefficient C_Q.

Effect of Oxygen Concentration

As can be observed from the different images in Fig. 3, the oxygen concentration has a significant effect on the luminosity of the flame and on the standoff distance but negligible changes on its shape. An increase in oxygen concentration results in a brighter flame, but the shape and transition point between the blue and yellow zone remain almost invariant. The effect of oxygen concentration on the flame shape is more significant for the lower velocity flames (Figs. 3a and 3b).

Characteristic temperatures obtained by means of the thermocouples placed at the trailing edge of the flame showed a temperature drop of approximately 300 K after the flame transitioned from normal to microgravity. Once the temperatures were established, an average value of the thermocouple giving the highest reading was used as characteristic flame temperature. Temperatures were corrected for radiation losses following the method of Fristrom and Westenberg.[34,35] Figure 4 shows the average temperatures as a function of the dimensionless volume ratio,[32] $C_Q = V_F / U_\infty$. The error bars show the maximum deviation from the average. Thermocouples perturb the flame; thus, these values can only be taken as characteristic values useful for relative comparison but clearly deviate from real flame temperatures. The error bars give an indication of the potential variations but do not provide an exact indication of the errors incurred in these measurements.

Figure 4 shows that the temperature is independent of C_Q but a strong function of the oxygen concentration. For $Y_O = 18\%$ the characteristic temperature is approximately 800 K for all values of C_Q and increases until it reaches approximately 1050 K for $Y_O = 50\%$.

Nonreactive Flow: Effect of Fuel-Injection Velocity

The preceding observations show that the flame geometry is controlled by fuel and oxidizer velocities and to a lower extent by the oxygen concentration. Flame temperature nevertheless seems to be only a function of the oxygen concentration. It is important to try to separate the influence of the flow structure and that of the exothermic reaction in order to get a better understanding of the characteristics of the flame. In this section an in-depth look at the structure of the flow will be presented in the context of the different flame regimes observed.

Structure of the Flow

The oxidizer and fuel flows were seeded independently to provide information on the mixing zone established between both flows. The diffusivity of the seeding particles is very low; therefore, their presence can only be attributed to convective transport. For each experimental condition a light sheet is used to illuminate the particles, and images are gathered independently for seeded fuel and seeded oxidizer. If the pictures are overlapped, three clear zones are established (Fig. 5): 1) one with no fuel (outer flow, $y > \delta_I$), with illuminated particles only when the oxidizer flow is seeded; 2) one with no oxidizer (inner flow, $y < \delta_E$), with illuminated particles only when the fuel flow is seeded; and 3) a mixing zone where fuel and oxidizer are present (shown gray in Fig. 5) shows illuminated particles for both cases, when fuel is seeded and when oxidizer is seeded.

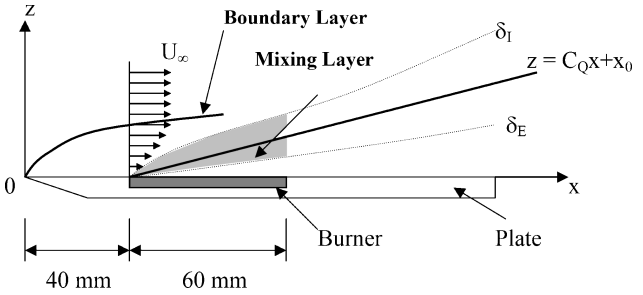

Fig. 5 Schematic of the flow structure showing the mixing zone and the internal and external flow boundaries.

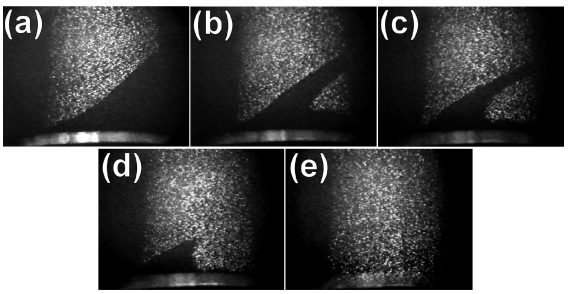

Fig. 6 Photographic images of an external flow seeded. The flow goes from the lest to the right on each picture: a) $y = 0$, b) $y = D/6$, c) $y = D/4$, d) $y = D/3$, and e) $y = D/2$, where D is the diameter of the burner (60 mm) and $y = 0$ corresponds to the center of the plate.

Close to the leading-edge determination of the frontier between the seeded and nonseeded flow is very difficult because of reflection of the light sheet on the burner; therefore, quantitative information will not always be presented for this zone.

A detailed tomography shows that fuel injection creates a three-dimensional flow structure where the oxidizer flow is blocked close to the leading edge and forced to move in the $-y$ and $+y$ directions. At the end of the injection zone, the oxidizer flow will move back toward the symmetry plane. Five planes of a series of tomographic images for a case where only the oxidizer flow was seeded are presented in Fig. 6 ($U_\infty = 23$ mm/s and $V_F = 4$ mm/s). Figure 6a shows that at the plane of symmetry the oxidizer is deflected upwards by the fuel leaving downstream an area absent of seeding particles. As the distance from the leading edge increases, an inflection point can be observed. As the light sheet is displaced from the axis of symmetry, toward the edge of the burner, particles can be traced in two different areas, and two borders between seeded and nonseeded areas appear (Fig. 6b). Figures 6c and 6d show that a further displacement of the light sheet from the axis of symmetry shows a decrease in the size of the zone lacking particles. The inflection point is no longer evident, and eventually the two seeded zones join inside the field of view of the camera. Finally, as the light sheet is brought to the edge of the burner the entire field shows a presence of seeding particles.

This shows clearly the presence of a three-dimensional flow pattern generated by the fuel injection. This three-dimensional flow structure was not observed for $V_F = 0$, where no recirculation zones are present above the burner, as confirmed by numerical simulation of the flow without injection.[31] The fuel injection acts as an obstacle to the oxidizer flow. Past this obstacle, the oxidizer can move back toward the plane of symmetry. This shows that the location of the flame will be strongly influenced by the flowfield resulting from the interaction of fuel and oxidizer.

By placing the laser sheet parallel to the x–y plane, $z = 10$ mm, a series of images corresponding to a top view of the burner were obtained (Figs. 7a and 7c), which confirmed the aforementioned

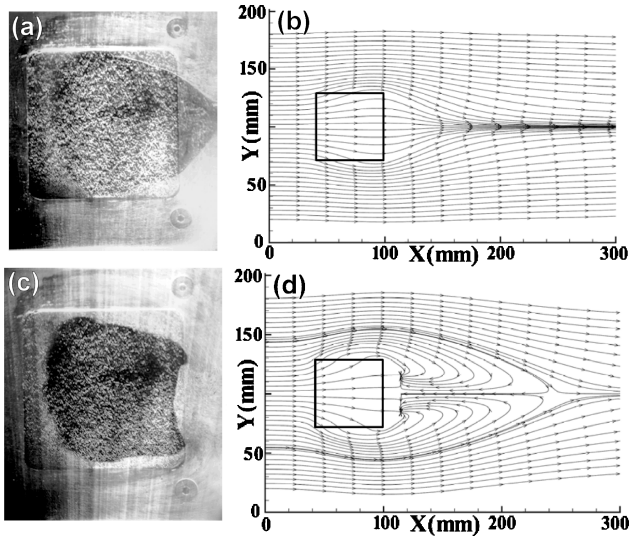

Fig. 7 Photographic images of an external flow seeded and corresponding numerical simulations. The laser sheet is placed parallel to the burner surface (x-y plane, $z = 10$ mm): a) flow visualization for $U_\infty =$ 100 mm/s, $V_f = 8$ mm/s; b) numerical streamlines for $U_\infty = 100$ mm/s, $V_f = 8$ mm/s; c) flow visualization for $U_\infty = 100$ mm/s, $V_f = 16$ mm/s; and d) numerical streamlines for $U_\infty = 100$ mm/s, $V_f = 16$ mm/s.

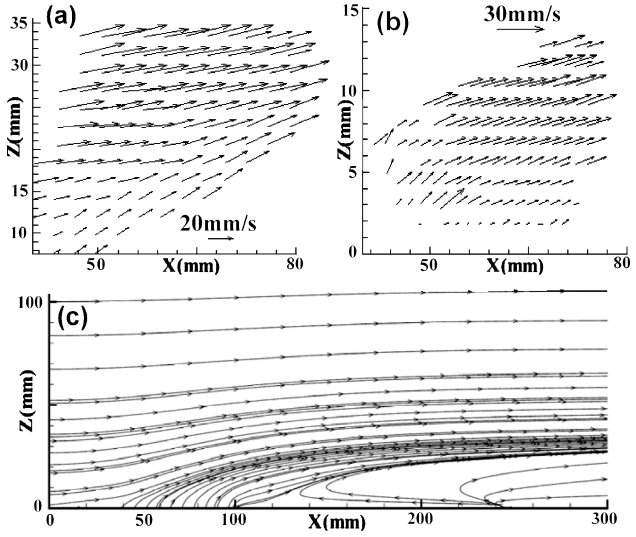

Fig. 8 Particle-image-velocimetry measurements for the plane of symmetry with $U_\infty = 20$ mm/s and $V_F = 3$ mm/s: a) external flow seeded, b) internal flow seeded, and c) streamlines in the symmetry plane of the plate extracted from numerical results, where $C_q = 0.16$, $U_\infty = 100$ mm/s, $V_f = 16$ mm/s.

observations, complemented by result from numerical simulations for the corresponding two cases (Figs. 7b and 7d). Figures 7a and 7b correspond to a freestream velocity significantly larger than the injection velocity, and Figs. 7c and 7d to injection and freestream velocities of comparable magnitude. The dimensionless volume coefficient C_Q, defined by Schlichting,[32] is considered to be the dominant parameter describing the effect of injection in boundary layers with blowing. Therefore, it will be used to define the flow regimes.

For Cq of the order of unity, the fuel injection displaces the oxidizer flow from the surface of the burner resulting in a recirculation zone at the trailing edge of the injection zone (Figs. 7a and 7b). A decrease in Cq (decrease in V_F or increase in U_∞) eliminates the recirculation zone, but the three-dimensional flow structure that brings the oxidizer toward the plane of symmetry persists (Figs. 7c and 7d). An increase Cq increases the particles-free area toward the trailing edge; thus, the oxidizer reaches the plane of symmetry further downstream.

Limitations on the size of the light sheet did not allow for a systematic determination of the downstream distance where tracer particles converged at the plane of symmetry, but numerical simulations indicated that the three-dimensional effect will be confined only to the burner edges if the ratio between injection and airflow velocities was smaller than 30 mm/s (Ref. 31).

Velocity Field

Quantitative characterization of the velocity field was done by means of particle image velocimetry. Figure 8a presents a characteristic case where only the oxidizer flow was seeded and Fig. 8b one where only the fuel flow contained particles. Both figures correspond to $U_\infty = 20$ mm/s and $V_F = 3$ mm/s. As the freestream approaches the leading edge, it is deflected upwards by the fuel injection. As can be seen in Fig. 8a, the vectors in the region upstream of the seeded area exceed the nominal 20 mm/s, revealing an acceleration of the flow. The origin of Fig. 8a is the leading edge of the porous plate, and vectors for $z < 8$ mm could not be defined because of poor seeding in this region. Figure 8b shows the vector field when the fuel is seeded.

The oxidizer stream accelerates the fuel flow until the particles exhibit a velocity comparable in magnitude to that of the external flow. No vectors could be obtained for $z < 4$ mm, but those obtained at $z = 4$ mm show characteristic velocities equivalent to those calculated by means of the mass flowmeters.

Velocity measurements in the present microgravity combustion chamber are very difficult; thus, only a few representative results can be obtained and are limited to a small window. Nevertheless, numerical simulations conducted for similar injection to freestream ratios serve to clarify the nature of the flowfield. Figure 8c shows the streamlines of one of such cases. As can be seen, the separation of the flow evidenced by the PIV measurements is very clear when observing the streamlines. The recirculation zone mentioned before follows the trailing edge of the burner.

The evolution of the velocity field as V_F and U_∞ were varied showed that both the deflection of the streamlines and the acceleration of the flow become less obvious as V_F decreases or U_∞ increases. Eventually, V_F will only affect the thickness of the boundary layer, but the flow will remain two dimensional close to the pane of symmetry.

Mixing Zone

A systematic evaluation of the effects of V_F and U_∞ on the structure of the flow was conducted by determining the borderline for seeded and nonseeded areas as a function of these parameters. All microgravity data presented in these sections were obtained during parabolic flights. Drop-tower test data were mostly used to validate the observations in the absence of g-jitter. The results are presented in Figs. 9a and 9b for the oxidizer seeded flow, or external flow δ_E, and fuel seeded flow, or internal flow (δ_I). The data are presented for two values of the dimensionless volume coefficient C_Q.

Figure 9a shows two extreme values of V_F (2 and 7 mm/s) for a constant value of $U_\infty = 20$ mm/s and Fig. 9b two extreme values of U_∞ (20 and 70 mm/s) for a constant value of $V_F = 7$ mm/s. The data show the expected result that for a constant V_F the magnitude of δ_E decreases when C_Q is reduced but does not correlate with this parameter. The magnitude of δ_I follows a similar dependency on C_Q than that of δ_E; again C_Q does not fully describe the evolution of δ_I. Overlapping of δ_E and δ_I provides an indication of the viscous layer and where fuel and oxidizer are present. Both figures show that a decrease in value of C_Q results in a decrease in the size of the mixing region (shaded area), which is approaching the surface of the burner. Further decrease of C_Q resulted in a mixing layer almost touching the surface of the burner ($C_Q < 0.001$). This corresponds well with the regime where blowing affects only fluid particles in the neighborhood of the wall.[31]

The preceding figures show the complexity of the flow above the burner. To separate the different elements contributing to the overall flow, the scaling of δ_E and δ_I will be done assuming the flow to be two dimensional. Although this has been shown not to be the case, it is a good way of determining under what conditions three-dimensional effects are important.

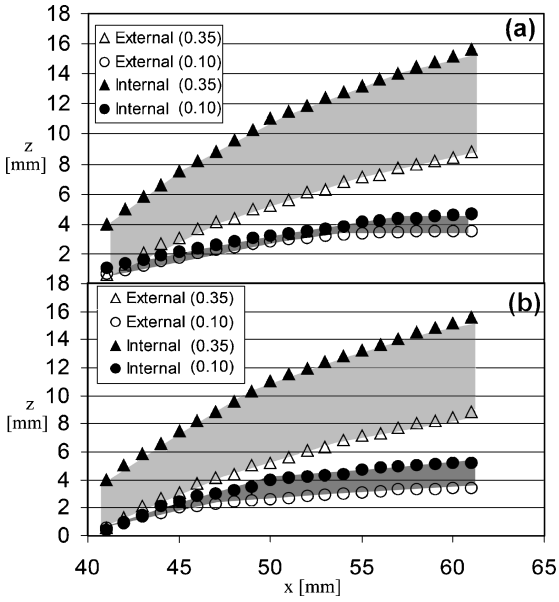

Fig. 9 Mixing zone for two extreme values of C_Q: a) constant U_∞ (20 mm/s) and two values of V_F (2 and 7 mm/s) and b) constant V_F (7 mm/s) and two values of U_∞ (20 and 70 mm/s).

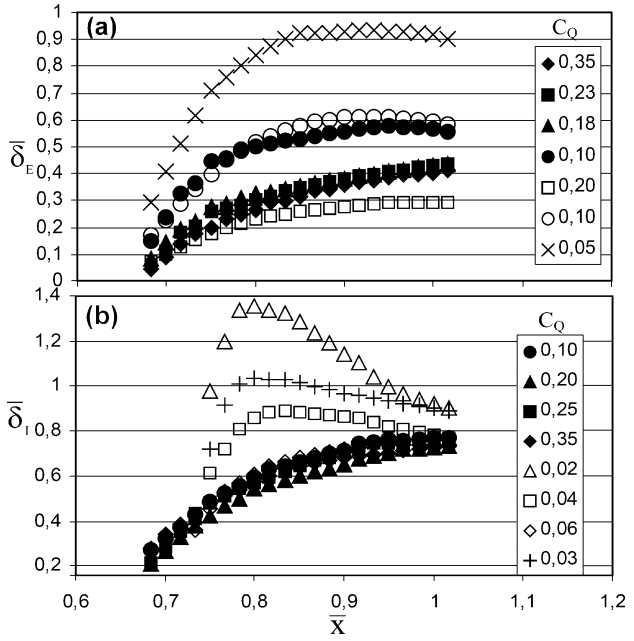

Fig. 10 Nondimensional boundary between seeded and unseeded flow as a function of the x coordinate normalized by the burner length L for different values of the dimensionless volume coefficient C_Q: a) internal flow seeded δ_I and b) external flow seeded δ_E.

There is no analytical solution to the problem of blowing in a boundary layer,[32] but, when C_Q is very large and the flow is separated, a stagnation plane can be defined. The locus of the stagnation plane is given by the equation[36]

$$z = C_Q x + x_0 \tag{1}$$

where $x_0 = 40$ mm for this burner. A schematic of this particular scenario is presented in Fig. 5. The viscous boundary layers will establish around this locus, and therefore δ_E will develop below this plane and δ_I above. Equation (1) being representative of the locus of the stagnation plane, for δ_E and δ_I all dimensions in the z direction will be scaled by $C_Q x$; therefore,

$$\bar{\delta}_E = \delta_E / C_Q x \tag{2}$$

$$\bar{\delta}_I = \delta_I / C_Q x \tag{3}$$

Scaling analysis will show that a developing region can be defined by the following expression:

$$x_C = \left(4/C_Q^2\right)(\nu/U_\infty) \tag{4}$$

and used as characteristic length scale in the x direction. Although the natural characteristic length scale for the x coordinate should be the initial length x_C, x_C falls within the area of interest only for $C_Q > 0.25$. For most of the experimental conditions, the region of interest is early in the developing region. Because the flow is far from being developed, the only adequate scale is the burner; thus, for Figs. 10a and 10b the nondimensional x coordinate is defined as

$$\bar{x} = x/L \tag{5}$$

where $L = 60$ mm for these particular experiments. Figure 10a shows $\bar{\delta}_E$ as a function of $\bar{x}$ and Fig. 10b, $\bar{\delta}_I$ as a function of $\bar{x}$. The results presented are only representative but serve to describe all different regimes.

The characteristic values used to scale both x and z coordinates seem adequate because the dependency on C_Q is properly described. For $C_Q > 0.15$ but $V_F < 4$ mm/s, the flow is fundamentally two dimensional, and $\bar{\delta}_E$ converges to a constant value ($C_Q = 0.20$ in Fig. 10a). For larger values of V_F, the dependency on C_Q is still well described, but $\bar{\delta}_E$ does not converge to a constant value but increases monotonically. The large injection velocity results in lateral entrainment that lifts the oxidizer away from the plate; for these conditions three-dimensional effects are of importance. These phenomena cannot be seen on $\bar{\delta}_I$, where all data converge to one single curve and toward a constant value for $C_Q > 0.06$. Although the internal flow seems to converge toward a sole solution for $C_Q > 0.06$, the external flow boundary converges only for $C_Q > 0.15$. The numerical simulations presented in Fig. 8c clearly show that $\bar{\delta}_E$ will fall within the region of flow acceleration, thus side entrainment (three-dimensional effects will be more important here). No three-dimensional effects trailing downstream seem obvious for $C_Q < 0.15$.

In summary, three different regimes have been identified; for $C_Q < 0.15$ the characteristics of the flowfield at the leading edge of the burner seem to have a significant effect on the mixing zone. This observation corresponds well with the study of Ha et al.[26] For $C_Q > 0.15$ two different regimes can be observed, for $V_F < 4$ mm/s the flow at the plane of symmetry is two dimensional and not affected by the side boundaries of the burner, and for $V_F > 4$ mm/s lateral entrainment results in a lift of the oxidizer boundary; this regime corresponds to the observations of Ramachandra and Raghunandan.[21] This work concentrates on the regime of $U_\infty < 150$ mm/s, which corresponds to the transition regime; previous work by Torero et al.[27] showed that for $U_\infty > 150$ mm/s the flame location converged to the two-dimensional boundary-layer solution hinting a similar convergence for the cold flow.

The values of C_Q that define the different regimes are given as a reference but cannot be generalized because only one single burner dimension was used for these experiments. Experiments with different burners are necessary to obtain quantitative criteria that define these different zones.

Analysis of the Reactive Flow

The flame standoff distance for $x < 60$ mm was studied. (The leading edge of the burner plate is at $x = 0$ and the porous plate at $x = 40$ mm.) The standoff distance is nondimensionalized as presented in Eqs. (2) and (3) and the x coordinate as shown by Eq. (5). The proposed scaling incorporates no density changes. This was done to isolate the effect of flow structure from thermal expansion, thus, being able to qualitatively show the importance of this effect. Proper estimation of the temperature fields could lead to a better scaling that incorporates thermal expansion, but the rough temperature estimates that could be obtained throughout this study do not provide a density field with enough certainty. The results are

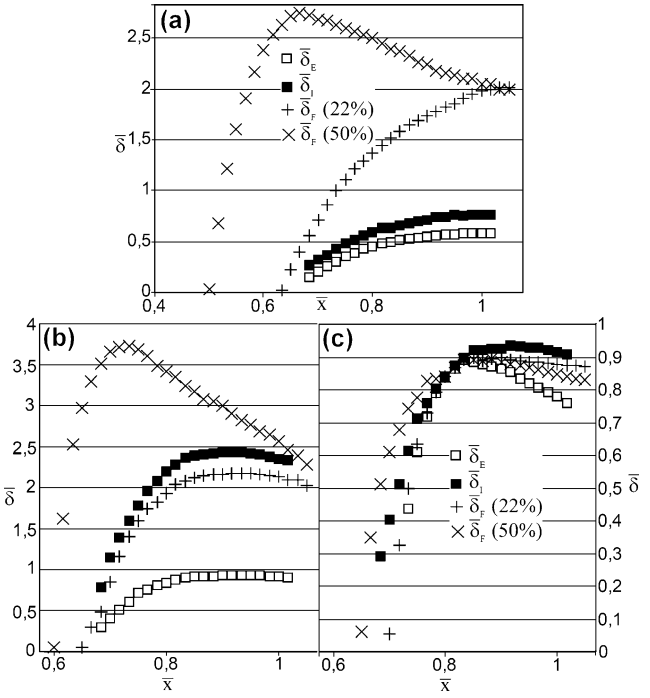

Fig. 11 Nondimensional flame standoff distance δ_F as a function of the x coordinate normalized by the burner length L as compared to $\bar{\delta}_I$ and $\bar{\delta}_E$: a) experimental conditions ($U_\infty = 20$ mm/s and $V_F = 2$ mm/s) corresponding to a case in region 1; b) experimental conditions ($U_\infty = 40$ mm/s and $V_F = 2$ mm/s) corresponding to a case in region 2; and c) experimental conditions ($U_\infty = 70$ mm/s and $V_F = 3$ mm/s) corresponding to a case in region 3.

presented in Figs. 11a, 11b, and 11c for characteristic cases corresponding to regions 1, 2, and 3, respectively (Fig. 2).

As already demonstrated, the characteristics of the flow are well represented by the scaling proposed by Eqs. (2), (3), and (5). If the flow density remained constant or density variations could be considered negligible, the flame will be placed inside the mixing layer. Inside the mixing zone, as the oxygen concentration increases the flame should approach the fuel-injection surface. Hirano et al.[19] and Hirano and Kanno[20] explained the velocity overshoots observed close to the flame as a consequence of thermal expansion caused by the exothermicity of the flame. Description of the flowfield has shown that, even in the absence of thermal expansion, velocity overshoots occur because of the interaction of the fuel and oxidizer flows. Although these results add an additional parameter to this particular scenario, they do not discard the effect that thermal expansion might have on the flowfield.

When fuel and oxidizer velocities are set such that the flame corresponds to region 1, the flame standoff distance $\bar{\delta}_F$ is much larger than $\bar{\delta}_E$ and $\bar{\delta}_I$, independent of the oxygen concentration. Figure 11a shows two representative cases for identical values of V_F and U_∞ but different oxygen concentrations (22 and 50%). The flame is not located inside the corresponding cold-flow mixing zone. This evidences a significant effect of thermal expansion under these flow conditions. The leading edge is displaced upstream from the mixing zone, and the discrepancy grows with the distance from the leading edge. An increase in oxygen concentration magnifies the discrepancy, which reaches a maximum at the leading edge of the porous plate. The coupling between thermal expansion and interacting flowfields gives a maximum perturbation at this point. Both the 22 and 50% flames converge to the same standoff distance as $\bar{x}$ increases. This shows that the flow is deflected at the leading edge by thermal expansion, but once this deflection has occurred, although the flow never comes back to its original streamlines, it gains the linear dependency with $\bar{x}$. This is similar to the cold flow, and under these conditions thermal expansion has no further effect. For $\bar{x} < 1$ the flame remains blue, and as thermal expansion becomes less important, $\bar{x} > 1$, the flame migrates toward a bright yellow color. The change in color is more obvious as the oxygen concentration increases, but its location (in $\bar{x}$) seems invariant with the oxygen concentration. The trajectory of soot particle migration has been mentioned earlier as a cause for the blue color of candle flames in microgravity.[7] When diffusion or thermal expansion dominates, soot particles cannot approach the flame, and, thus, the flame is blue. When convection, natural or forced, carries soot toward the flame, it becomes incandescent and glows or burns, and the flame becomes yellow. This simple explanation seems to describe well the present experimental observations.

As V_F and U_∞ increase and the flame enters region 2 the effect of thermal expansion becomes less obvious (Fig. 11b). For low oxygen concentration, thus lower temperatures, the flame enters the cold-flow mixing zone. For higher oxygen concentrations, higher temperatures, the flame remains outside the cold-flow mixing zone close to the leading edge. Eventually, $\bar{x} > 1$, the 50% flame also enters the mixing zone. Again, in this region thermal expansion becomes less important, and $\bar{x} \approx 1$ corresponds to the location where the flame transitions from blue toward yellow. In this case, an increase in oxygen concentration still leads to a larger standoff distance showing the lesser importance of diffusion as compared to expansion and convection.

Finally, for region 3, Fig. 11c shows that close to the leading edge the flames are outside the cold-flow mixing zone, but very close downstream of the leading edge of the porous plate, $\bar{x} \approx 0.8$, the flame penetrates the mixing zone. The discrepancies, even close to the leading edge, are very small compared to regions 1 and 2. For $\bar{x} < 0.8$, thermal expansion dominates, and hotter flames (50%) have a larger standoff distance than colder flames (22%). Under these conditions the flame is blue. For $\bar{x} > 0.8$, a higher oxygen concentration results in a smaller standoff distance denoting the importance of diffusion. At this point fuel and oxidizer are transported toward the mixing zone by convection, but within this zone diffusion determines the flame location. Under these conditions the flame is yellow.

For all three regions, in the zone in which thermal expansion is dominant, scaling the measured value of $\bar{\delta}_F$ by means of the ratio between the temperature of the flame and the ambient temperature brings the standoff distance to a value comparable to that of $\bar{\delta}_E$ and $\bar{\delta}_I$. This observation, although a very approximate one, gives further strength to the preceding phenomenological explanations.

Numerical simulations incorporating the combustion reaction confirmed the preceding observations.[31] The peak energy release zone was established as the locus of the flame. Comparison between the numerical results and experimental standoff distances to validate the accuracy of these numerical simulations has been presented by Rouvreau et al.[31] and will not be repeated here. The numerical simulations help to emphasize the impact that the flame exothermicity has on the standoff distance and can be used to discuss the influence of density changes on the flame location.

Conclusions

An experimental study of a low-Reynolds-number diffusion flame has been conducted to provide further insight on the structure of diffusion flames representative of fire in microgravity. The flow conditions, $18\% < Y_O < 22\%$, $V_F \approx 5$ mm/s, and $U_\infty < 150$ mm/s, have been set to correspond well to a potential fire onboard of a spacecraft. A gas fuel (ethane) injected through a porous burner has been chosen to simulate a condensed fuel.

Flow visualization has shown that a three-dimensional flow pattern is introduced by the injected flow resulting in separation of the oxidizer flow and a mixing zone detached from the porous plate. The mixing zone approaches the plate when increasing the Reynolds number and when decreasing the injection velocity. The flow characteristics correspond to a transitional regime but can be adequately scaled by convection controlled characteristic variables.

Three characteristic regimes have been identified: for $C_Q < 0.15$, the flowfield at the leading edge of the burner has a significant effect on the mixing zone. For $C_Q > 0.15$ and $V_F < 4$ mm/s, the flow at the plane of symmetry is two dimensional and not affected by the side boundaries of the burner. For $C_Q > 0.15$, and $V_F > 4$ mm/s, lateral

entrainment results in a lift of the oxidizer boundary, and therefore the physical boundaries of the burner have an effect on the structure of the mixing zone.

This work concentrates on the regime of $U_\infty < 150$ mm/s, which corresponds to the transition regime, but previous work showed that for $U_\infty > 150$ mm/s the flame location could be scaled in a consistent manner thus hinting a similar convergence for the cold-flow.

Experiments in microgravity have shown that a minimum fuel-injection velocity is necessary for the flame to be stable. For low flow velocity (both V_F and U_∞) thermal expansion plays a dominant role on the flame geometry and flowfield. As both fuel and oxidizer velocities increase, the importance of thermal expansion is reduced to the leading edge. The experimental results presented can be generalized in what concerns the qualitative explanations of the phenomena. Quantitative results are only given as a reference but should not be extrapolated to different experimental conditions. Precise local velocity and temperature (or density) measurements on the reacting flow are necessary to obtain quantitative boundaries for the different regimes presented in this work.

These results are valid only for gaseous fuel and oxidizer and should not be directly extrapolated to condensed fuel burning. Nevertheless, the general conclusions apply in a qualitative manner to condensed fuel burning. Constant fuel injection uses an average velocity at the surface; therefore, when compared to condensed fuel vaporization, has a stronger effect on the structure of the flow downstream of the leading edge and weaker close to the leading edge. Because fuel injection forces separation of the freestream close to the leading edge the present experimental observations raise many unanswered questions related to how fuel and oxidizer are transported toward the reaction zone that are general to all low-momentum nonpremixed flames.

Acknowledgments

This work was funded by ESA and the Centre National d'Etudes Spatiales. Funding for J.L.T. came from the Minta Martin Research Fellowship. The authors thank Olivier Minster and Bernard Zappoli for their support.

References

[1]Ross, H. D., *Fire in Free Fall: Micro-Gravity Combustion*, Academic Press, San Diego, CA, 2001, pp. 299–418.

[2]Friedman, R., "Fire Safety Practices and Needs in Human-Crew Spacecraft," *Journal of Applied Fire Safety*, Vol. 2, No. 3, 1992–93, pp. 243–259.

[3]Friedman, R., "Fire Safety in Spacecraft," *Fire and Materials*, Vol. 20, No. 5, 1996, pp. 235–243.

[4]Ross, H. D., "Burning To Go: Combustion of Orbit and Mars," Eastern States Sec. of the Combustion Inst., Invited Lecture 5, Oct. 1997.

[5]Torero, J. L., Bahr, N. J., and Carman, E. J., "Assessment of Material Flammability for Micro-Gravity Environments" International Astronautical Federation, Paper 97-J.2.02, Oct. 1997.

[6]T'ien, J. S., "The Possibility of a Reversal of Material Flammability Ranking from Normal Gravity to Microgravity," *Combustion and Flame*, Vol. 80, No. 3–4, 1990, pp. 355–357.

[7]Law, C. K., and Faeth, G. M., "Opportunities and Challenges of Combustion in Micro-Gravity," *Progress in Energy and Combustion Science*, Vol. 20, No. 1, 1994, pp. 65–113.

[8]Ronney, P. D., "Understanding Combustion Processes Through Microgravity Research," *Proceedings of the Combustion Institute*, Vol. 27, 1998, pp. 2485–2506.

[9]Emmons, H., "The Film Combustion of Liquid Fuel," *Zeitschrift für Angewandte Mathematik und Mechanik*, Vol. 36, 1956, pp. 60–71.

[10]Fernandez-Pello, A. C., *Combustion Fundamentals of Fire: The Solid Phase*, Academic Press, Boston, 1995, Chap. 2.

[11]Pagni, P. J., and Shih, T. M., "Excess Pyrolyzate," *16th Symposium (International) on Combustion*, Combustion Inst., Pittsburgh, PA, 1976, pp. 1329–1343.

[12]Lavid, M., and Berlad, A. L., "Gravitational Effects on Chemically Reacting Boundary Layer Flows over a Horizontal Flat Plate," *16th Symposium (International) on Combustion*, Combustion Inst., Pittsburgh, PA, 1976, pp. 1157–1568.

[13]Fernandez-Pello, A. C., and Pagni, P. J., "Mixed Convective Burning of a Vertical Fuel Surface," *Proceedings of the 1983 ASME–JSME Thermal Engineering Joint Conference*, Vol. 4, 1983, pp. 295–301.

[14]Chen, C. H., and T'ien, J. S., "Diffusion Flame Stabilization at the Leading Edge of a Fuel Plate," *Combustion Science and Technology*, Vol. 50, 1986, pp. 238–306.

[15]Mao, C. P., Kodama, H., and Fernandez-Pello, A. C., "Convective Structure of a Diffusion Flame over a Flat Combustible Surface," *Combustion and Flame*, Vol. 57, No. 2, 1984, pp. 209–236.

[16]Kodama, H., Miyasaka, K., and Fernandez-Pello, A. C., "Extinction and Stabilization of a Diffusion Flame on a Flat Combustible Surface with Emphasis on Thermal Controlling Mechanisms," *Combustion Science and Technology*, Vol. 53, 1987, pp. 37–50.

[17]Drysdale, D., *An Introduction to Fire Dynamics*, Wiley, New York, 1985, pp. 226–252.

[18]DeRis, J., and Orloff, L., "The Role of Buoyancy, Direction and Radiation on Turbulent Diffusion Flames on Surfaces," *Fifteenth Symposium (International) on Combustion*, Combustion Inst., Pittsburgh, PA, 1974, pp. 175–182.

[19]Hirano, T., Iwai, K., and Kanno, Y., "Measurement of the Velocity Distribution in the Boundary Layer over a Flat Plate with a Diffusion Flame," *Astronautica Acta*, Vol. 17, 1972, pp. 811–818.

[20]Hirano, T., and Kanno, Y., "Aerodynamic and Thermal Structures of the Laminar Boundary Layer over a Flat Plate with a Diffusion Flame," *Fourteenth Symposium (International) on Combustion*, Combustion Inst., Pittsburgh, PA, 1973, pp. 391–398.

[21]Ramachandra, A., and Raghunandan, B. N., "Investigations on the Stability and Extinction of a Laminar Diffusion Flame over a Porous Flat Plate," *Combustion Science and Technology*, Vol. 36, 1984, pp. 109–121.

[22]Andreussi, P., and Petarca, L., "Film Combustion of Ethyl Alcohol in a Parallel Air Stream," *Eighteenth Symposium (International) on Combustion*, Combustion Inst., Pittsburgh, PA, 1981, pp. 1861–1869.

[23]Andreussi, P., "Modelling of Laminar Diffusion Flames over a Horizontal Plate," *Combustion and Flame*, Vol. 45, 1982, pp. 1–6.

[24]Andreoti, S., Andreussi, P., and Petraca, L., "Boundary Layer Burning of Fuel Surfaces: Thermal and Aerodynamic Structure of the Flame," *Combustion Science and Technology*, Vol. 40, 1984, pp. 279–291.

[25]Nakagawa, Y., Nishiwaki, N., and Hirata, M., "Effect of Combustion on a Laminar Boundary Layer," *Thirteenth Symposium (International) on Combustion*, Combustion Inst., Pittsburgh, PA, 1971, pp. 813–819.

[26]Ha, J. S., Shim, S. H., and Shin, H. D., "Boundary Layer Diffusion Flame over a Flat Plate in the Presence and Absence of Flow Separation," *Combustion Science and Technology*, Vol. 75, 1991, pp. 241–260.

[27]Torero, J. L., Bonneau, L., Most, J. M., and Joulain, P., "The Effect of Gravity on a Laminar Diffusion Flame Established over a Horizontal Flat Plate," *25th Symposium (International) on Combustion*, Combustion Inst., Pittsburgh, PA, 1994, pp. 1701–1709.

[28]Torero, J. L., Bonneau, L., Most, J. M., and Joulain, P., "On the Geometry of Laminar Diffusion Flames Established over a Flat Plate Burner," *Advances in Space Research*, Vol. 16, No. 7, 1995, pp. 149–152.

[29]Torero, J. L., Wang, H.-Y., Joulain, P., and Most, J.-M., "Flat Plate Diffusion Flames: Numerical Simulation and Experimental Validation for Different Gravity Levels," *Lecture Notes in Physics*, Vol. 464, 1995, pp. 401–413.

[30]McGrattan, K. B., Baum, H. R., Rehm, R. G., Hamins, A., Forney, G. P., and Floyd, J. E., "Fire Dynamics Simulator—Technical Reference Guide (Ver. 2)," National Inst. of Standards and Technology, 2001.

[31]Rouvreau, S., Joulain, P., Wang, H. Y., Cordeiro, P., and Torero, J. L., "Numerical Evaluation of Boundary Layer Assumptions Used for the Prediction of the Stand-off Distance of a Laminar Diffusion Flame," *Proceedings of the Combustion Institute*, Vol. 29, 2002, pp. 2527–2534.

[32]Schlichting, H., *Boundary Layer Theory*, 7th ed., McGraw–Hill, New York, 1979.

[33]David, L., "Developpements d'une Technique d'Analyse Quantitative Automatisee en Ecoulements Tridimensionnels," Ph.D. Dissertation, Dept. of Fluid Mechanics, Univ. de Poitiers, Poitiers, France, 1996.

[34]David, L., Texier, A., Fayolle, J., and Jay, J., "Three PIV Technique Comparisons in Hydrodynamic Flows," *4th Asian Symposium on Visualisation*, edited by Q. D. Wei, International Academic Publishers, Beijing, 1996, pp. 273–276.

[35]Fristrom, R. M., and Westenberg, A. A., *Flame Structure*, Series in Advanced Chemistry, McGraw–Hill, New York, 1965.

[36]Jones, J. W., Isaacson, L. I., and Vreekes, S., "A Turbulent Boundary Layer with Mass Addition, Combustion, and Pressure Gradients," *AIAA Journal*, Vol. 9, No. 9, 1971, pp. 1762–1768.

C. Kaplan
Associate Editor